Multi-Objective Optimal Design and Analysis of Variable Leakage Flux IPM Motors for Improve Flux-Weakening Ability

Xiping Liu, Gaosheng Guo*, Longxin Du, and Wenjian Zhu

Abstract—In this paper, two variable leakage flux permanent magnet (VLFPM) machines are proposed. The keys are to adopt the rotor with single-layer and double-layer PMs and intentionally create leakage flux paths to extend the operating speed range and increase the machine efficiency. The characteristics of the variable leakage flux of the proposed machines are investigated. In order to improve the performances of the VLFPM machines, the Multi-Objective Genetic Algorithm (MOGA) method is applied for achieving the multi-objective optimizations of variables. Then, the performances of the double-layer permanent magnet variable leakage flux motor (DLPM-VLFM) and the single-layer permanent magnet variable leakage flux motor (SLPM-VLFM) are analyzed and compared with conventional interior PM machine (CIPMM) in detail. The performances mainly include flux linkage and torque, flux-weakening capability and efficiency. Finally, it is shown by analysis and comparison that the DLPM-VLFM can have a wider range of speed and high efficiency.

1. INTRODUCTION

With the problem of environmental pollution and energy consumption [1], interior permanent magnet synchronous motor (IPMSM) has become one of the electrical machines which is widely used in the traction motors of electric vehicles (EVs) and hybrid EVs (HEVs), electric aircraft, and industrial application due to high torque density, high power density, and high efficiency [2–4]. In order to meet the demand for PMSM in application, variable flux machines (VFM) are investigated. Generally, to achieve a wide speed range, large d-axis current is applied to weaken the PM flux. However, it is inevitable that more copper loss will be produced, and the risk of irreversible demagnetization of PM will be increased [5–7]. Besides, the speed range may be limited due to the limitations of maximum current and voltage for the inverter.

In the past few years, great attention has been paid to find some valid methods to obtain a wider speed range for the motors. In [8–10], some flux-intensifying interior permanent magnet (FI-IPM) motors with the unique characteristic of d-axis inductances L_d larger than that of q-axis inductances L_q are proposed. As a result, the positive reluctance torque can be obtained at a positive d-axis current, and the lower risk of irreversible demagnetization of the PMs can be achieved. Besides, the flux-weakening capability can be improved because of the flux-intensifying effect. Hence, the wider speed range of the FI-IPM motor compared with some IPMSMs with the characteristic of $L_d > L_q$ can be realized. In [11–13], variable flux memory motor (VFMM) has been proposed. Since s low coercive-force (LCF) PM is applied in VFMM, the LCF-PM magnetization strength can be controlled by injecting d-axis current pulses to remagnetize or demagnetize. The flux controllability of VFMM can be easily achieved to widen the speed range. Mechanical variable flux motor (MVFM) is introduced in [14–16]. The machine equips a mechanical flux-adjusting device to self-activating the change of air-gap flux density.

The lower loss and wider speed range of the MVFM can be obtained. Those methods can be effectively applied to achieve variable flux by unique characteristics, PM material, and mechanical device.

In this paper, the proposed machines employ a different method to flux-weakening by intentionally creating a leakage flux path, which is a narrow path linked to two tops of adjacent poles [17–19]. The leakage flux can be controlled by q-axis current. Thus, the purpose of variable flux is achieved. Generally, there are two main designing strategies for expanding the variable flux range: applying a better leakage flux way and widening the path. However, the types of flux leakage are limited and need further research. A wider path approach can obtain a more extensive range of variation, but the requirement for a larger current to obtain torque at low speeds will lower performance. In [20], different rotor topologies for high-performance traction machine applications are compared. Therefore, DLPM-VLFM and SLPM-VLFM are designed to realize variable leakage flux. And the leakage flux path is applied in the two motors.

To obtain a satisfactory performance of machines, multi-objective optimization methods have been widely applied in recent research. In [21], multi-objective optimization based on a nondominated sorting genetic algorithm (NSG-II) is adopted to optimize selected key parameters of the machines. In [22], structural parameters of the motor are optimized by adopting dual-level response surface methodology and Booth's algorithm. In [23], an IPMSM is optimized by combining genetic algorithm (GA) with the coarse mesh finite element method. These optimization methods can effectively improve the performance of the motor. In this paper, the MOGA is used to optimize the two motors.

The paper is organized as follows. The initial design of the topology and operating principle of the proposed VLFM are described. The final model of the two proposed motors is determined by adopting the multi-objective optimization method to optimize some selected key parameters. The electromagnetic performances of the two proposed motors are comprehensively evaluated based on two-dimensional finite element analysis (2DFEA) and compared with the CIPMM. Moreover, the flux-weakening ability, speed range, and efficiency are compared and analyzed. Finally, the conclusion is given, and the performance of the DLPM-VLFM can be proved better through analysis and comparison.

2. TOPOLOGY AND PRINCIPLES OF MACHINE

2.1. Machine Topology

In Figure 1, the rotor topology evolution from the conventional interior PM motor to the SLPM-VLPM and DLPM-VLPM is depicted, including the evolution of the q-axis magnetic barriers and PMs. As seen from the figure, to realize the characteristic of the variable leakage flux, the leakage flux bypass is set on the q-axis of the two proposed motors. To improve the air-gap flux density, the PMs of the DLPM-VLFM are divided into two layers. Besides, the machines with three-phase, 48 slots and 8 pole configuration, and distributed winding are adopted for the stator.

The SLPM-VLFM and DLPM-VLFM are PM brushless (PMBL) motors, so the initial design of the two proposed motors can be obtained according to the design theory of PMBL motors. The corresponding size equation of the two proposed motors can be expressed as:

$$D_{si}^2 L_{axis} = \frac{2P_c}{\pi^2 k_{wd} n_s B_{fr} A_m \eta \cos \varphi} \tag{1}$$

where D_{si} is the inner diameter of the stator, L_{axis} the active stack length, P_c the output power, π the efficiency, k_{wd} the winding factor, n_s the rated speed, A_m the electrical load, B_{fr} the effective value of the air-gap flux density, and φ the power factor angle.

According to the design requirements listed in Table 1, the initial size specifications of the three types of motors can be calculated and listed in Table 2.

2.2. Operation Principles

The speed of the motor can be expressed as:

$$\omega = \frac{U}{p\sqrt{(\psi_m + L_d i_d)^2 + (L_q i_q)^2}} \tag{2}$$
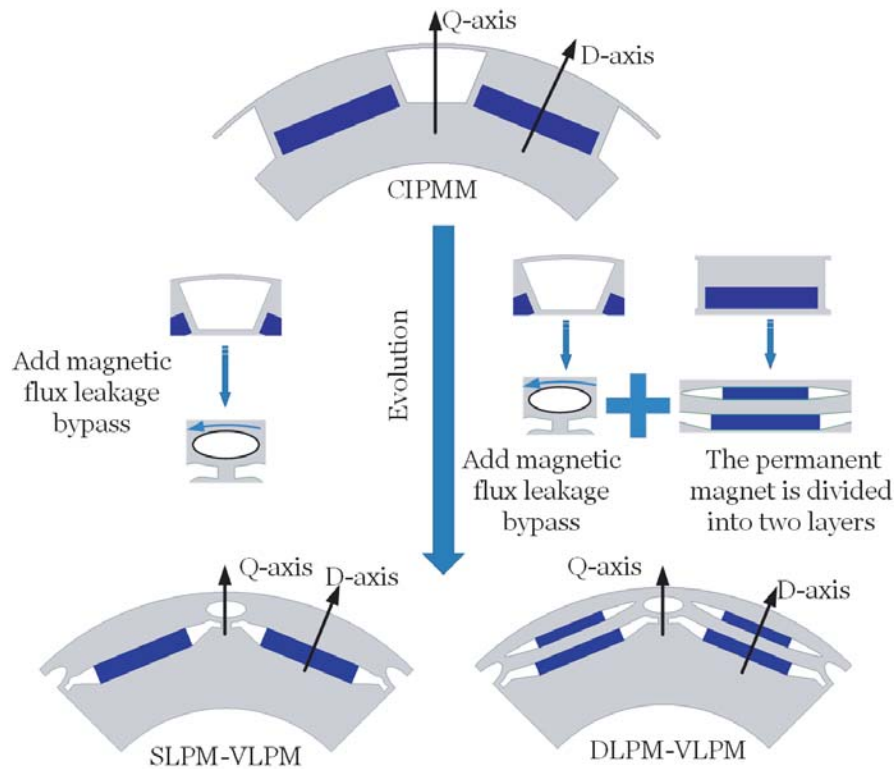
Figure 1. Rotor evolution from the conventional interior PM motor to the SLPM-VLPM and the DLPM-VLPM.

Table 1. Design requirements of the motors.

Items	Requirements
Rated power (kW)	10
Rated voltage (V)	240
Rated speed (rpm)	1200
Rated output torque (Nm)	≥ 60

Table 2. Initial key parameters of the three motors.

Items	values
Stator inner diameter D_{si} (mm)	161.9
Air-gap length (mm)	0.75
Active stack length L_{axis} (mm)	83.82
Numbers of turns	18
PM material	N36Z_20 (1.03 T, 920 kA/m)
Total PM volume (mm^3)	136794.24

where p is the number of pole pairs; i_d and i_q are the currents of the d-axis and q-axis, respectively; Ψ_m is the flux linkage provided by PMs; U is the terminal voltage of the motor. According to Equation (2), the speed range is constrained because the voltage and current of the PM machine are limited. When

the voltage and armature current of the motor reaches the maximum value; the current has only a d-axis current component ($i_{lim} = i_d$, $i_q = 0$ A); and the influence of stator resistance is ignored, the speed reaches the ideal maximum. The expression is as follows:

$$\omega_{\max} = \frac{U_{lim}}{p(\Psi_m - L_d i_{lim})} \tag{3}$$

where U_{lim} and i_{lim} are the maximum voltage and maximum armature current, respectively. According to Eq. (3), the speed range can be extended by increasing d-axis inductance and decreasing Ψ_m. The proposed motors achieve flux-weakening by controlling Ψ_m.

For analyzing the variable leakage flux principles of the SLPM-VLFM and DLPM-VLFM, the magnet paths of the three motors with no load are shown in Figures 2(a), (b), and (c). The flux weakening through the designed magnetic flux leakage path can be achieved due to the unique structure of the two proposed motors.
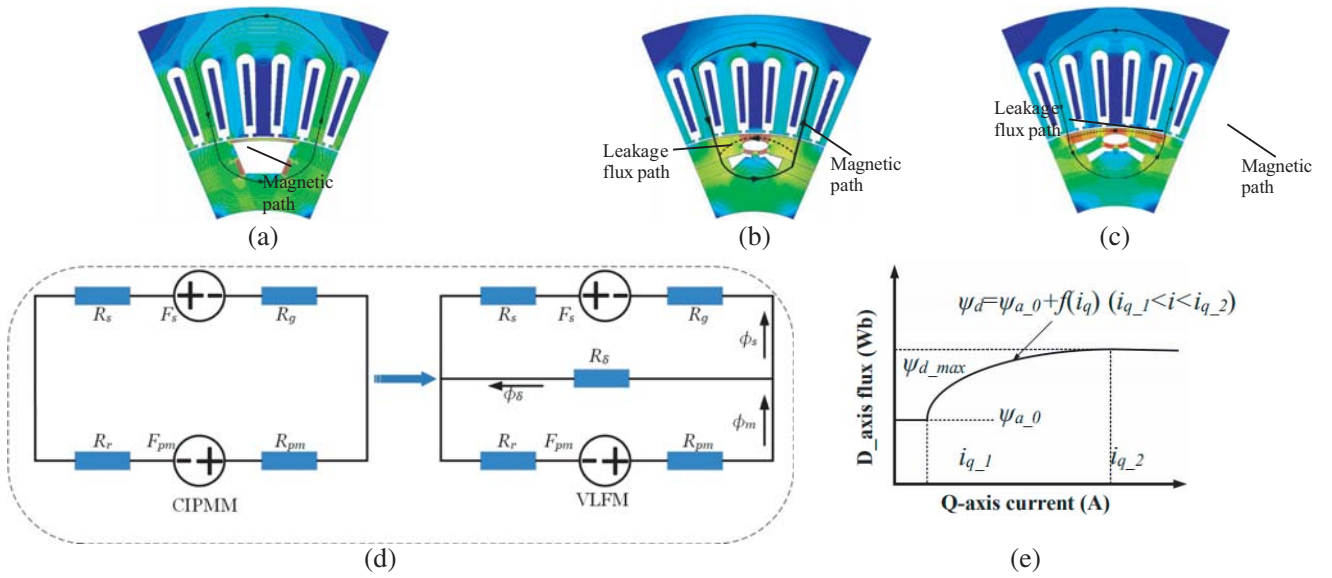
Figure 2. Theoretical analysis for variable leakage flux. (a) Magnetic path of CIPMM. (b) Magnetic path of SLPM-VLFM. (c) Magnetic path of DLPM-VLFM. (d) Magnetic equivalent circuit. (e) Variable flux property.

Figure 2(d) shows the equivalent magnetic circuit for the motors. It can be found that the main difference between the proposed motors and the CIPMM is the magnetic leakage loop. According to the figure, the expressions for the magnet circuit are given as follows:

$$\begin{cases} \begin{bmatrix} \phi_s \\ \phi_m \end{bmatrix} = \frac{A}{|A|} \begin{bmatrix} F_s \\ F_{pm} \end{bmatrix} \\ A = \begin{bmatrix} R_\delta + R_r + R_{pm} & R_\delta \\ R_\delta & R_s + R_g + R_\delta \end{bmatrix} \\ |A| = (R_\delta + R_s + R_{pm})(R_s + R_g + R_\delta) - R_\delta^2 \end{cases} \tag{4}$$

The magnetomotive force of PMs and armature reaction force are F_{pm} and F_s, respectively; R_r, R_{pm}, R_δ, R_g, R_s are the reluctances of rotor, PM, bypass, air-gap, stator, respectively; φ_s, φ_δ, φ_m are the magnetic fluxes of stator, bypass, PM, respectively.

$$\begin{cases} \phi_\delta = \phi_m - \phi_s = \dfrac{(R_g + R_s) F_{pm} - R_s F_s}{R_\delta (R_r + R_{pm}) + (R_\delta + R_r + R_{pm})(R_s + R_g)} \\ R_\delta = \dfrac{l}{u(iq)s} \end{cases} \tag{5}$$

where l, s, and $u(iq)$ are the length, cross-sectional area, and permeability of the bypass, respectively. According to the above formula, the reluctance of the leakage flux path can be increased to change the leakage flux because of the larger q-axis current.

According to Equation (6), when i_d is 0 A, Ψ_d is equal to Ψ_m. Thus, the change of PM flux linkage Ψ_m can be well analyzed by analyzing the relationship between d-axis flux linkage Ψ_d and d-axis current i_d. Besides, for further analyzing the principle of variable leakage flux, the relationship between q-axis current and d-axis flux Ψ_d can be clearly described by Figure 2(e) in which Ψ_{a_0} is the magnet flux with no load, $f(i_q)$ a function of the magnet flux and q-axis current, and i_{q_2} the boundary current. According to Figure 2(e), Equation (7) can be obtained. When i_q is less than i_{q_1}, the current has little effect on the reluctance of bypass, so the flux is almost unchanged. When i_q is greater than i_{q_1}, the reluctance of bypass will increase gradually of bypass, and the leakage flux will decrease. Finally, the leakage flux will reach the minimum, and the d-axis flux linkage is maximum when i_q reaches i_{q_2}.

$$\begin{cases} \Psi_d = \Psi_m + L_d i_d \\ \Psi_d(i_d = 0\,\text{A}) = \Psi_m \end{cases} \tag{6}$$

$$\Psi_d = \begin{cases} \Psi_{a\_0}, & 0 \leq i \leq i_{q\_1} \\ \Psi_{a\_0} + f(i_q), & i_{q\_1} \leq i_q \leq i_{q\_2} \\ \Psi_{d\_\max}, & i_q \geq i_{q\_2} \end{cases} \tag{7}$$

To sum up, the magnet flux of the bypass will be changed due to the variation of the current and magnetic resistance of the q-axis. It means that leakage flux can be adjusted by controlling the q-axis current.

2.3. Configuration Optimization of Machine

To improve the performance of the proposed machines, the optimization of the proposed machines is necessary. The multi-objective optimization flowchart of the VLFM is described in Figure 3, which includes the following steps:

Step 1: Initial design of the VLFM. According to the design theory of the IPMSM and the design requirements of the proposed machine, the dimensions of the initial specifications of the proposed machines can be obtained. The design variables are selected to establish the parametric model. Besides, according to application requirements, the optimization objectives are determined.

Step 2: Parameters sensitivity analysis. The sensitivity $S(x_i)$ of each selected design variable on optimization objectives is defined. Analyze the influence of each parameter on the optimization objective.

Step 3: Multi-objective optimization. The optimization model of the machines is presented. The MOGA optimization method is adopted to determine the final value of the design variables.

Step 4: Performance evaluation. In this section, the electromagnetic performances of the motors are analyzed.

According to design requirements, some parameters are selected for optimization. The parametric models of the two proposed motors are shown in Figure 4. The selected design parameters and the corresponding range of variation are given in Table 3.

In addition, the output torque T_r, torque ripple T_{ripple}, and flux-weakening coefficient $\Delta\Psi$ are selected as the optimization objectives to improve the electromagnetic performance of the output torque and flux-weakening ability of the proposed motors.

The torque ripple and flux-weakening coefficient are defined as follows:

$$T_{ripple} = \frac{T_{r\_\max} - T_{r\_\min}}{T_{r\_avg}} \tag{8}$$

$$\Delta_\Psi = \frac{\Psi_{d\_\max} - \psi_{a\_0}}{\psi_{d\_\max}} \tag{9}$$

where $T_{r\_\max}$, $T_{r\_\min}$, T_{r_avg} are the maximum, minimum, and average values of the torque, respectively. To analyze the influence of these selected parameters on the optimization objectives, sensitivity analysis
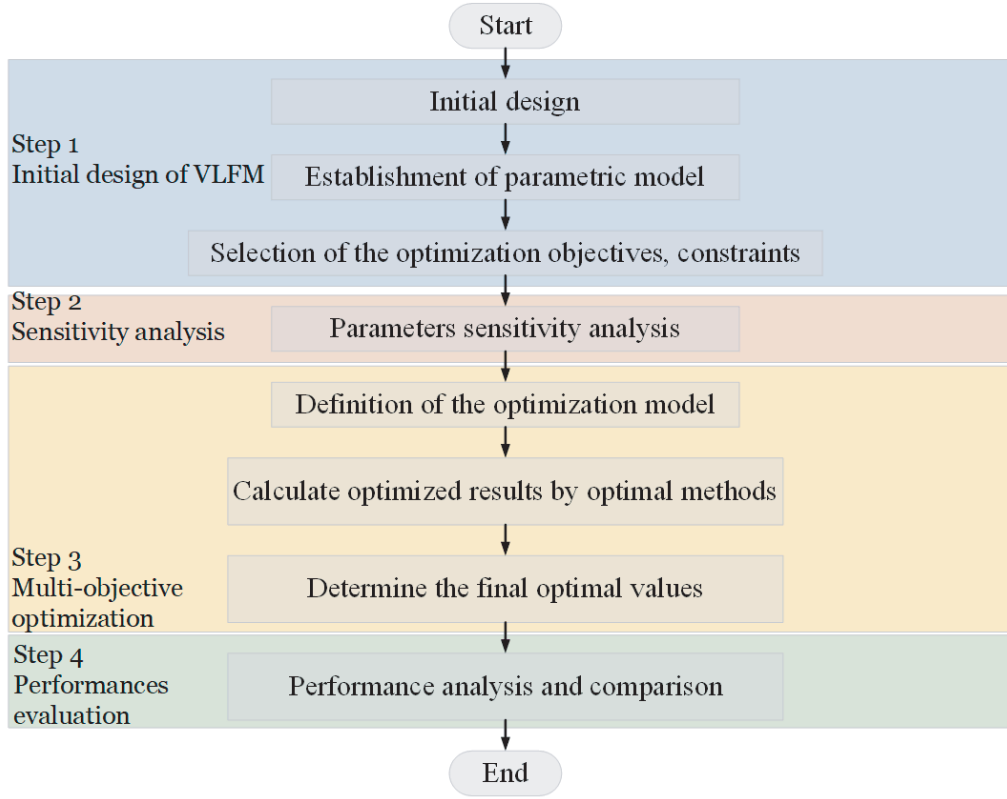
Figure 3. The flowchart of the multi-objective optimization approach.
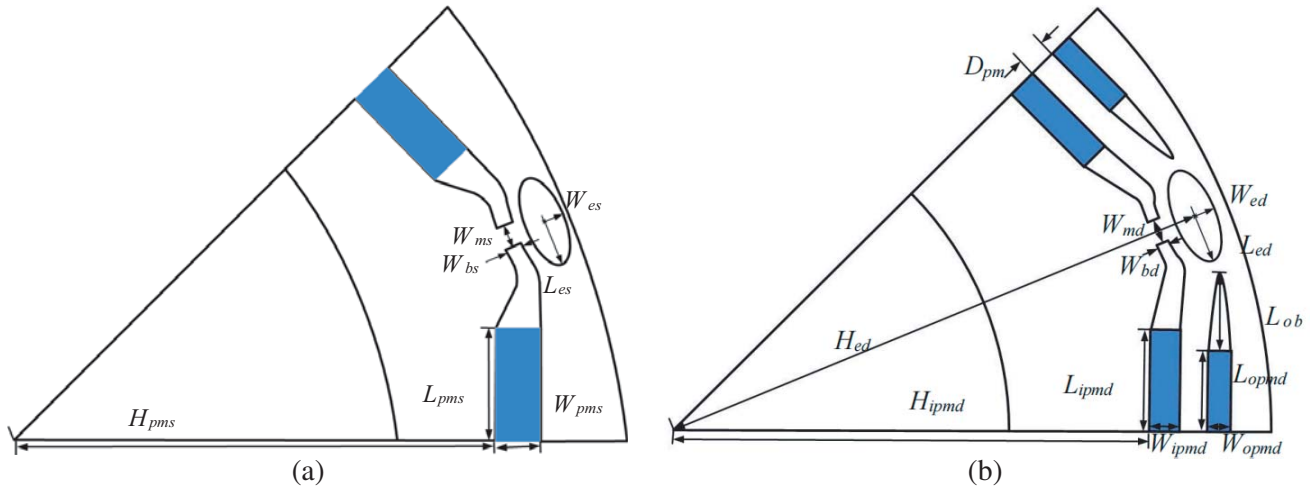
Figure 4. Parametric model. (a) SLPM-VLFM. (b) DLPM-VLFM.

is used in this paper, where the corresponding sensitivity index is given in Eq. (10).

$$S_i = \frac{V\left(E(y|x_i)\right)}{V(y)} \tag{10}$$

where y is the optimization objective; x_i $(i = 1, 2, 3 \ldots, n)$ is the selected design variables; $E(y/x_i)$ is the average value of y when x_i is constant; $V(E(y/x_i))$ is the variance of $E(y/x_i)$; and $V(y)$ is the variance of y. A positive sensitivity index indicates that the optimization objective will increase with the increase of design variable, whereas a negative one means a contrary variation. The greater absolute value of

Table 3. Variation range of the selected variables.

Motors	Design variables	Variation ranges
SLPM-VLFM	PM height H_{pms} (mm)	[60, 65]
	PM length L_{pms} (mm)	[14, 17]
	PM width W_{pms} (mm)	[5, 7]
	Elliptic magnetic barrier width W_{es} (mm)	[2, 3]
	Elliptic magnetic barrier length L_{es} (mm)	[4, 8]
	Magnetic barrier width W_{bs} (mm)	[1, 4]
	Magnetic bridges width W_{ms} (mm)	[2, 5]
DLPM-VLFM	Inside PM height H_{ipmd} (mm)	[61, 65]
	Inside PM length L_{ipmd} (mm)	[12, 16]
	Inside PM width W_{ipmd} (mm)	[3, 5]
	Outside PM length L_{opmd} (mm)	[6, 13]
	Outside PM width W_{opmd} (mm)	[2, 4]
	Elliptic magnetic barrier height H_{ed} (mm)	[74.5, 76]
	PMs distance D_{pm} (mm)	[2, 5]
	Outside magnetic barrier length L_{obd} (mm)	[8, 13]
	Magnetic bridges width W_{md} (mm)	[2, 5]
	Inside magnetic barrier width W_{bd} (mm)	[1, 4]
	Elliptic magnetic barrier width W_{ed} (mm)	[2, 3]
	Elliptic magnetic barrier length L_{ed} (mm)	[4, 8]

the sensitivity index means that the design variable has more impact on the optimization objectives. According to Equation (10), the sensitivity index of each variable on the optimization objectives can be calculated, as shown in Figure 5. In Figure 5(a), it can be seen that the height H_{spm}, length L_{pms}, and width W_{pms} of the PM and the long axis L_{es} and short axis W_{es} of the elliptic magnetic barrier have relatively great influence on the optimization objectives. In Figure 5(b), it can be observed that the
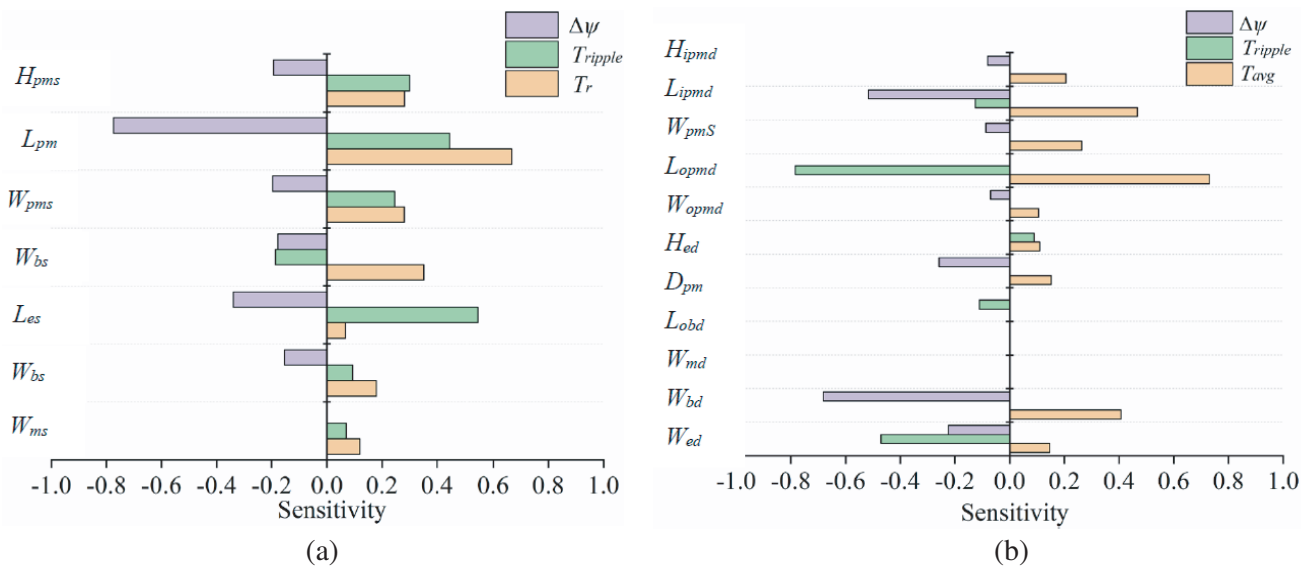
Figure 5. Sensitivity analysis. (a) SLPM-VLFM. (b) DLPM-VLFM.

parameters of the PMs and elliptic magnetic barrier have large sensitivity values. It means that these variables have a larger impact on the optimization objectives.

In order to obtain the better performance of the two proposed motors, the boundary constraints are set as

$$T_r \geq 60\,\mathrm{Nm}; \quad T_{ripple} \leq 0.15; \quad \Delta\Psi \geq 0.25 \tag{11}$$

The MOGA is adopted for the two proposed motors to optimize variables. The optimization results of the two machines are shown in Figure 6, where the optimal point can be obtained efficiently based on the boundary constraints. The final values of the design variables of the two machines are listed in Table 4.

(a)   (b)
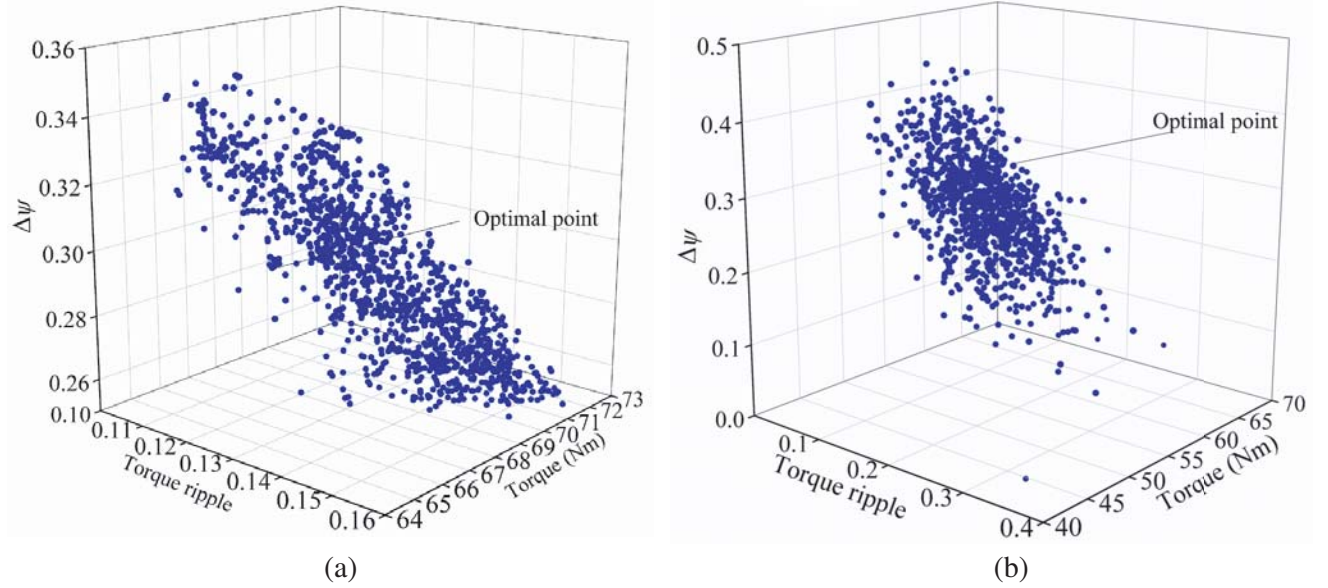
Figure 6. Optimization results of the two proposed motors. (a) SLPM-VLFM. (b) DLPM-VLFM.

3. ELECTROMAGNETIC PERFORMANCES ANALYSIS

3.1. Back-EMF and Flux Linkage of Machines

In Figure 7(a), the no-load back-EMF waveform of the three motors is shown at the speed of 2000 rpm. It can be observed that the magnitudes of the back-EMF differ significantly; the back-EMF of the two proposed motors are much smaller than that of the CIPMM, indicating that the magnetic field of the proposed motors can be effectively weakened. Figure 7(b) shows the Fourier Transformation results of back-EMF waveforms. It can be clearly found that the high harmonic component of the DLPM-VLFM is smaller than that of the SLPM-VLFM and CIPMM. It means that the DLPM-VLFM is easier to control due to more sinusoidal back electromotive force waveforms.

The flux linkage distributions with no-load and load are shown in Figures 8(a), (b), and (c). In Figure 8(a), under the no-load and load condition, the flux of CIPMM changes very little. In Figures 8(b) and (c) under the no-load condition, most of the magnet flux of adjacent magnetic poles form loops pass leakage flux bypass without passing through the stator. Under the load condition, the magnet flux path is toward the stator teeth path instead of the bypass between magnet poles due to the influence of i_q. The d-axis fluxes of the three motors at different q-axis currents are given in Figure 8(d). It can be found that the d-axis flux of the SLPM-VLFM and DLPM-VLFM is increased by injecting q-axis current. And the variable flux range of DLPM-VLFM is about 29.0%, which is slightly larger than that of SLPM-VLFM of 26.8%. Besides, the maximum d-axis flux of DLPM-VLFM is also slightly greater than SLPM-VLFM. The d-axis flux of the CIPMM is larger than that of SLPM-VLFM and

Table 4. The final values of the design variables.

Motors	Parameters	Unit	Initial values	Optimal values
SLPM-VLFM	H_{pms}	mm	63	63.469
	L_{pms}	mm	15	16.053
	W_{pms}	mm	6	6.843
	W_{es}	mm	2.5	2.8761
	L_{es}	mm	6	4.1389
	W_{bs}	mm	2	2.187
	W_{ms}	mm	1.5	2.3604
DLPM-VLFM	H_{ipmd}	mm	63.92	63.806
	L_{ipmd}	mm	13.68	14.806
	W_{ipmd}	mm	4	4.4032
	L_{opmd}	mm	10.8	10.911
	W_{opmd}	mm	3.2	3.4032
	H_{ed}	mm	75	75.552
	D_{pm}	mm	3.72	2.8952
	L_{obd}	mm	11	11.508
	W_{md}	mm	1.5	1.8423
	W_{bd}	mm	22	24.105
	W_{ed}	mm	2.5	2.4476
	L_{ed}	mm	6	5.1936
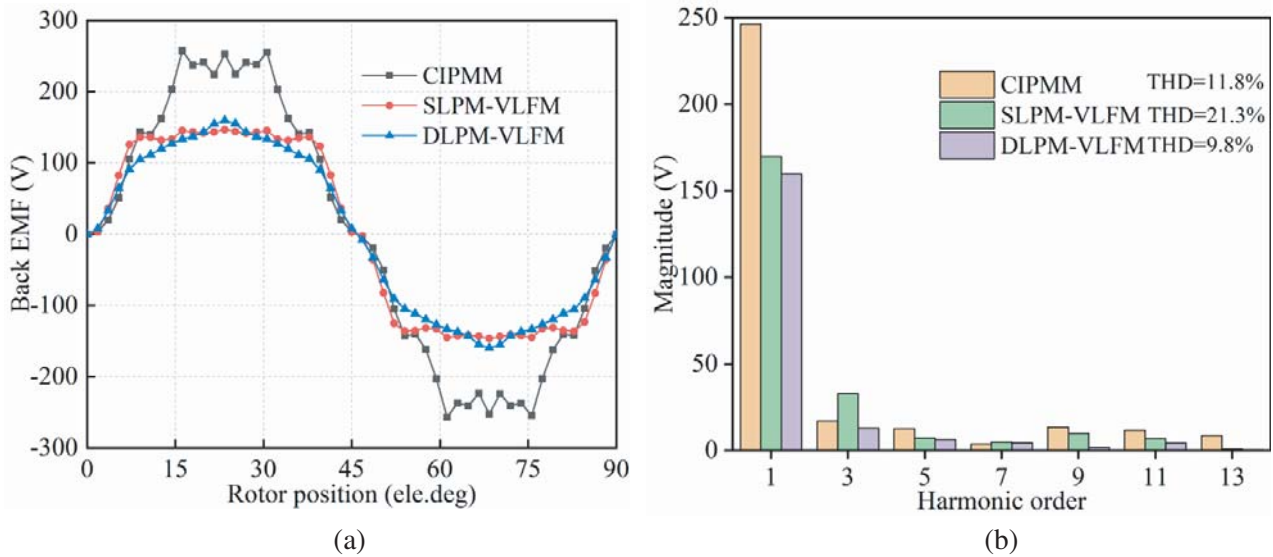
Figure 7. No-load back-EMF of the three motors. (a) Waveforms. (b) Harmonic component.

DLPM-VLFM, even though the d-axis flux of CIPMM is reduced with the current increase. It indicates that the high torque can be easily achieved for CIPMM.

Based on the above analysis, the d-axis flux of the SLPM-VLFM and DLPM-VLFM can be changed by injecting i_q, which verifies the effectiveness of the various leakage flux method. The various flux ranges are an important standard to evaluate the flux-weakening capability of VFM, so it can predict that the flux-weakening capability of the two proposed motors is better than that of the CIPMM.
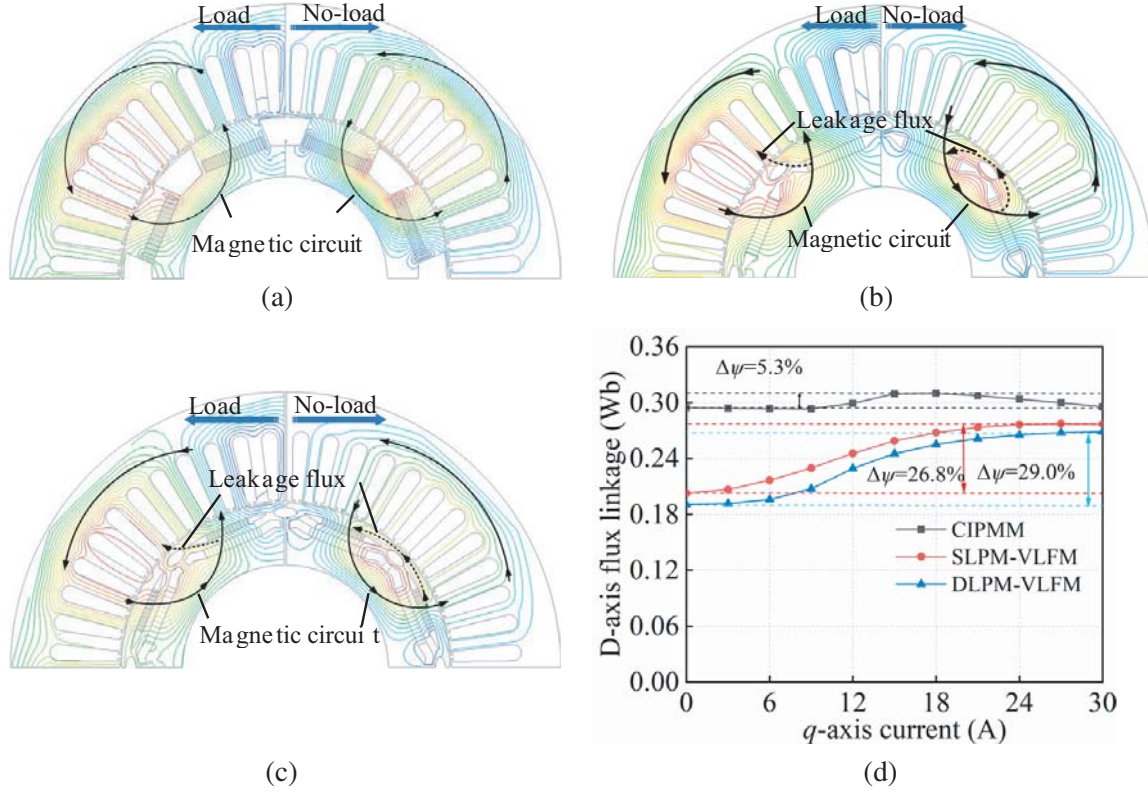
Figure 8. Flux characteristics. (a) Flux characteristics of CIPMM. (b) Flux characteristics of SLPM-VLFM. (c) Flux characteristics of DLPM-VLFM. (d) Relationship between q-axis current and d-axis flux linkage.

3.2. Torque Characteristics

The electromagnetic torque of the IPMSM can be expressed as:

$$T = \frac{3P}{2} \left[\Psi_m i_q + (L_d - L_q) i_d i_q \right] \tag{12}$$

According to Equation (12), the torque characteristics of the three types of motors are analyzed. The torque of the three types of motors at different current angles are shown in Figure 9(a). It can be found that the maximum torque of the CIPMM is higher than that of the SLPM-VLFM and DLPM-VLFM, which mainly results from the bigger flux linkage in the CIPMM. Moreover, Figure 9(b) shows the comparison of torque waveforms for the three motors with maximum torque operating conditions. As seen from the figure, the torque ripple of the CIPMM is higher than that of the two proposed motors.

3.3. Flux-Weakening Ability

The proposed motor is designed to achieve a wider range of speeds, so it is necessary to study the flux weakening ability of the motor and the characteristics of torque and output power with the variation of speed.

The flux-weakening ability can be analyzed according to Equation (13); the flux-weakening ability of the three motors is given in Table 5. It can be seen that the flux-weakening ability of the two proposed motors is higher than that of the CIPMM.

$$I_{ch} = \frac{\Psi_m}{L_d (I_d = I_{\lim}, \ I_q = 0 \, \text{A})} \tag{13}$$
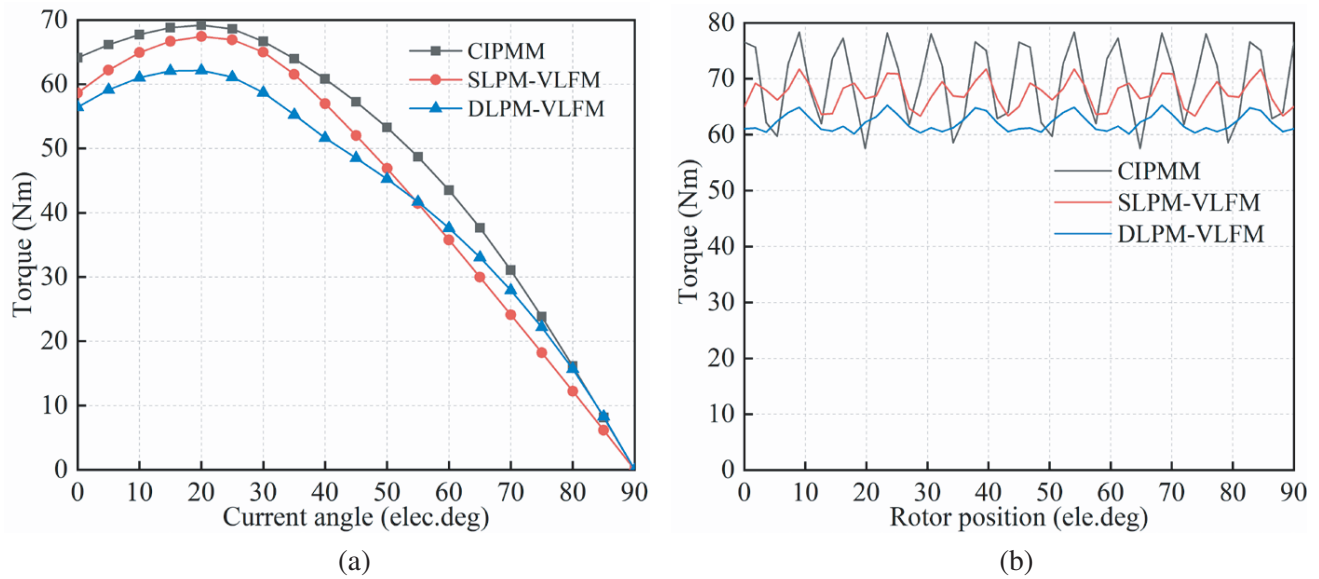
Figure 9. Torque characteristics of the three motors. (a) Torque versus current angles. (b) Output torque versus rotor position.

Table 5. Parameters of flux-weakening ability.

Items	CIPMM	SLPM-VLFM	DLPM-VLFM
PM flux linkage Ψ_m (Wb)	0.29	0.203	0.18
d-axis inductance L_d (mH)	7.67	18.3	17.14
Characteristic current I_{ch} (A)	37.8	11.1	10.5
Rated current I_{lim} (A)	25	25	25
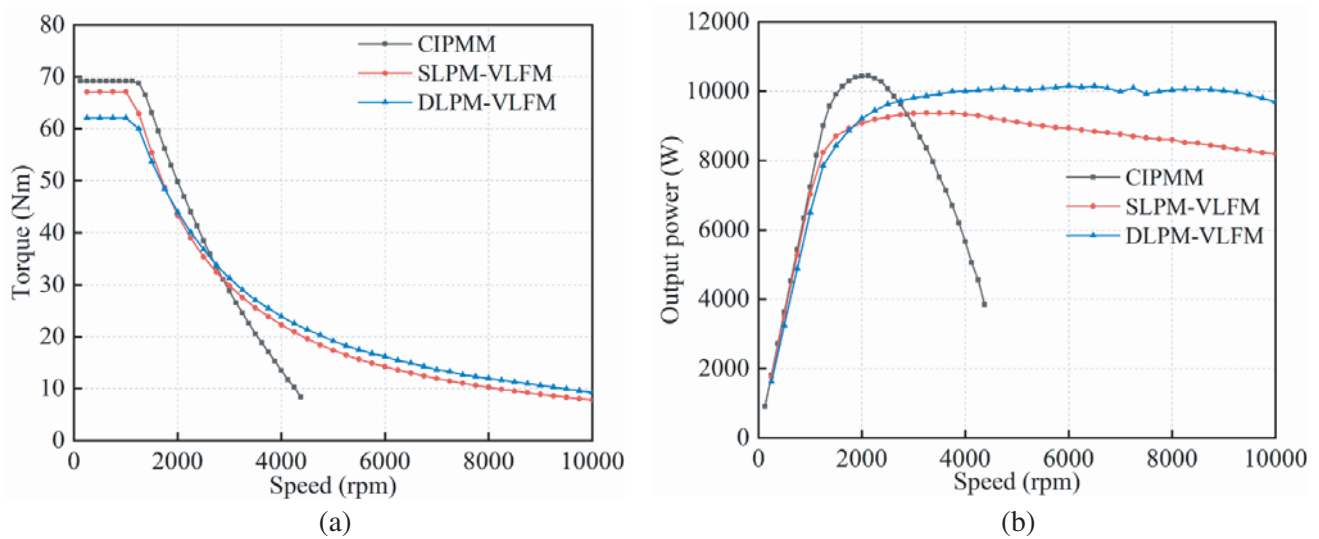
Figure 10. Performance comparisons of the three motors. (a) Torque-speed envelops. (b) Output power-speed envelops.

The torque and output power versus speed curves of the three types of motors are shown in Figures 10(a) and (b), respectively. From the two figures, it can be found that the maximum output torque and output power of the CIPMM are slightly larger than that of the SLPM-VLFM and DLPM-VLFM. The two proposed motors possess a wider speed range and constant power range than that of the CIPMM due to the variable leakage flux characteristics. Moreover, the constant-power region, output torque, and output power of the DLPM-VLFM are greater than that of SLPM-VLFM in the high-speed due to better flux-weakening ability.

According to the above analysis, the speed range of the two proposed motors is much larger than that of CIPMM. It means that the speed range of the motor can be extended by variable leakage flux.

3.4. Efficiency

Figures 11(a), (b), and (c) show the efficiency maps of CIPMM SLPM-VLFM and DLPM-VLFM, respectively. The efficiency of the three types of motors is analyzed as follows.
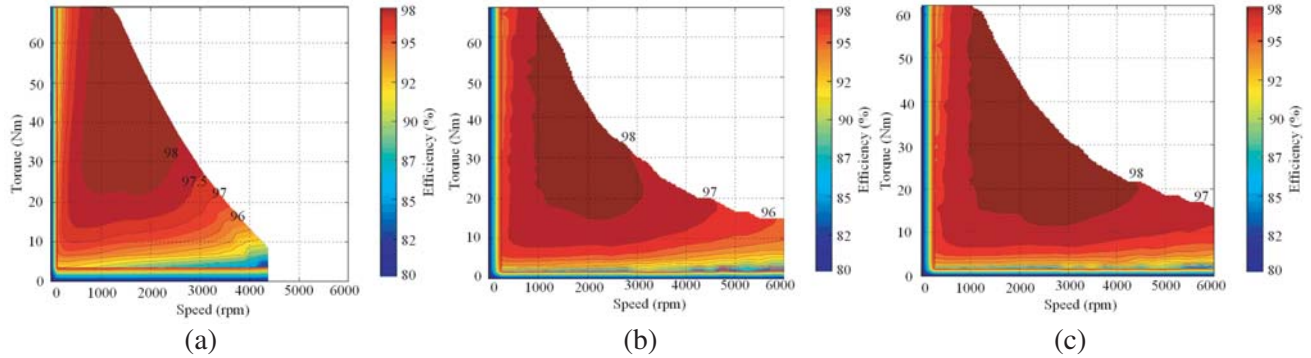
Figure 11. Efficiency maps of the three motors. (a) CIPMM. (b) SLPM-VLFM. (c) DLPM-VLFM.

In Figure 11(a), it can be found that the high-efficiency area of the CIPMM is in the speed range about 700 rpm to 2500 rpm. At high speed, the efficiency of the CIPMM declined sharply, because the air-gap magnetic field of the CIPMM is difficult to regulate.

Comparing the three figures, it is found that the 98% and 97% efficiency areas of the two proposed motors are greater than that of CIPMM, because the variable leakage flux characteristic of the two proposed motors can reduce the core loss and flux-weakening current. Besides, it can be seen that the high-efficiency area of the DLPM-VLFM is far larger than that of the SLPM-VLFM, because flux-weakening ability is better, and the air gap magnetic field has lower harmonic content.

4. CONCLUSION

In this paper, SLPM-VLFM and DLPM-VLFM are proposed to realize variable flux linkage by leakage flux bypass. The initial models and variable leakage flux principle of the two motors are investigated. An optimization method is performed for the two proposed motors to improve the flux-weakening ability and output torque. The electromagnetic performances of the three types of motors are analyzed by 2DFEM. The results show that the speed range and high-efficiency area of the two proposed motors are larger than that of CIPMM. It indicates that the variable flux leakage method can effectively widen the speed range and increase the high-efficiency area. Considering the comprehensive performance, DLPM-VLFM is the best among the three motors.

ACKNOWLEDGMENT

REFERENCES

1. Cao, R. W., C. Mi, and M. Cheng, "Quantitative comparison of flux-switching permanent-magnet motors with interior permanent magnet motor for EV, HEV, and PHEV applications," *IEEE Transactions on Magnetics*, Vol. 48, No. 68, 2374–2384, 2012.

2. Kakosimos, P. E., A. G. Sarigiannidis, M. E. Beniakar, A. G. Kladas, and C. Gerada, "Induction motors versus permanent-magnet actuators for aerospace applications," *IEEE Transactions on Industrial Electronics*, Vol. 61, No. 8, 4315–4325, 2014.

3. Yang, Y. Y., S. M. Castano, R. Yang, M. Kasprzak, B. Bilgin, A. Sathyan, H. Dadkhah, and A. Emadi, "Design and comparison of interior permanent magnet motor topologies for traction applications," *IEEE Transactions on Transportation Electrification*, Vol. 3, No. 1, 86–97, 2017.

4. Yang, Z., F. Shang, I. P. Brown, and M. Krishnamurthy, "Comparative study of interior permanent magnet, induction, and switched reluctance motor drives for EV and HEV applications," *IEEE Transactions on Transportation Electrification*, Vol. 1, No. 3, 245–254, 2015.

5. Jang, J., M. Humza, and B. Kim, "Design of a variable-flux permanent-magnet synchronous motor for adjustable-speed operation," *IEEE Transactions on Industry Applications*, Vol. 52, No. 4, 2996–3004, 2016.

6. Kim, K.-C., "A novel magnetic flux weakening method of permanent magnet synchronous motor for electric vehicles," *IEEE Transactions on Magnetics*, Vol. 48, No. 11, 4042–4045, 2012.

7. Kohara, A., K. Hirata, N. Niguchi, and Y. Ohno, "Finite-element analysis and experiment of current superimposition variable flux machine using permanent magnet," *IEEE Transactions on Magnetics*, Vol. 52, No. 9, 18–25, 2016.

8. Kato, T., N. Limsuwan, C. Y. Yu, K. Akatsu, and R. D. Lorenz, "Rare earth reduction using a novel variable magnetomotive force flux-intensified IPM machine," *IEEE Transactions on Industry Applications*, Vol. 50, No. 3, 1748–1756, 2014.

9. Limsuwan, N., Y. Shibukawa, D. D. Reigosa, and R. D. Lorenz, "Novel design of flux-intensifying interior permanent magnet synchronous machine suitable for self-sensing control at very low speed and power conversion," *IEEE Transactions on Industry Applications*, Vol. 47, No. 5, 2004–2012, 2011.

10. Zhu, X. Y., W. Y. Wu, S. Yang, Z. X. Xiang, and L. Quan, "Comparative Design and analysis of new type of flux-intensifying interior permanent magnet motors with different q-axis rotor flux barriers," *IEEE Transactions on Energy Conversion*, Vol. 33, No. 4, 2260–2269, 2018.

11. Hua, H., Z. Q. Zhu, A. Pride, R. Deodhar, and T. Sasaki, "Comparative study on variable flux memory machines with parallel or series hybrid magnets," *IEEE Transactions on Industry Applications*, Vol. 55, No. 2, 1408–1419, 2019.

12. Hua, H., Z. Q. Zhu, A. Pride, R. P. Deodhar, and T. Sasaki, "A novel variable flux memory machine with series hybrid magnets," *IEEE Transactions on Industry Applications*, Vol. 53, No. 5, 4396–4405, 2017.

13. Liu, F. L., L. M. Cheng, M. Q. Wang, G. Y. Qiao, P. Zheng, and H. Yang, "Comparative study of hybrid-PM variable-flux machines with different series PM configurations," *AIP Advances*, Vol. 9, No. 12, 321–332, 2019.

14. Elloumi, N., M. Bortolozzi, A. Masmoudi, M. Mezzarobba, M. Olivo, and A. Tessarolo, "Numerical and analytical approaches to the modeling of a spoke type IPM machine with enhanced flux weakening capability," *IEEE Transactions on Industry Applications*, Vol. 55, No. 5, 4702–4714, 2019.

15. Liu, X., T. Sun, Y. Zou, C. Huang, and J. Liang, "Modelling and analysis of a novel mechanical-variable-flux IPM machine with rotatable magnetic poles," *IET Electric Power Applications*, Vol. 14, No. 11, 2171–2178, 2020.

16. Tessarolo, A., M. Mezzarobba, and R. Menis, "Modeling, analysis, and testing of a novel spoke-type interior permanent magnet motor with improved flux weakening capability," *IEEE Transactions on Magnetics*, Vol. 51, No. 4, 1–10, 2015.

17. Aoyama, M., and T. Noguchi, "Study and experimental performance evaluation of flux intensifying PM motor with variable leakage magnetic flux," *Electrical Engineering In Japan*, Vol. 207, No. 4, 36–54, 2019.

18. Kato, T., M. Minowa, H. Hijikata, K. Akatsu, and R. D. Lorenz, "Design methodology for variable leakage flux IPM for automobile traction drives," *IEEE Transactions on Industry Applications*, Vol. 51, No. 5, 3811–3821, 2015.

19. Kusase, S. and K. Kurihara, "A proposal for a new variable leakage flux motor with interpolar gap and permanent magnets," *IEEJ Journal of Industry Applications*, Vol. 6, No. 6, 381–386, 2017.

20. Wang, A., Y. Jia, and W. L. Soong, "Comparison of five topologies for an interior permanent-magnet machine for a hybrid electric vehicle," *IEEE Transactions on Magnetics*, Vol. 47, No. 10, 3606–3609, 2011.

21. Ma, Y., T. W. Ching, W. N. Fu, and S. Niu, "Multi-objective optimization of a direct-drive dual-structure permanent magnet machine," *IEEE Transactions on Magnetics*, Vol. 55, No. 10, 1–4, 2019.

22. Asef, P., R. B. Perpiñà, M. R. Barzegaran, A. Lapthorn, and D. Mewes, "Multiobjective design optimization using dual-level response surface methodology and Booth's Algorithm for permanent magnet synchronous generators," *IEEE Transactions on Energy Conversion*, Vol. 33, No. 2, 652–659, 2018.

23. Nakata, T., M. Sanada, S. Morimoto, and Y. Inoue, "Automatic design of IPMSMs using a genetic algorithm combined with the coarse-mesh FEM for enlarging the high-efficiency operation area," *IEEE Transactions on Industrial Electronics*, Vol. 64, No. 12, 9721–9728, 2017.